Design and experiment of split-type tracked chassis applied in hilly and mountainous regions

Wei Wang[1†], Lin Yuan[1,2†], Guolong Li[1], Shiji Zhang[1], Tiejun Wang[1*], Chuanyin Tang[3*]

(1. *College of Engineering, Shenyang Agricultural University, Shenyang 110866, China*;
2. *College of Intelligent Manufacturing, Xinjiang Vocational University of Technology, Kashgar 844004, China*;
3. *College of Mechanical Engineering and Automation, Northeastern University, Shenyang 110819, China*)

Abstract: The terrain in hilly and mountainous regions is characterized by its discontinuity, constant undulations, and complex environment, leading to significant vibrations and potential tipping over of operating machinery. Traditional crawler chassis face challenges when encountering uneven terrain, with one side possibly being suspended and causing tipping. This study introduces a crawler chassis with a split structure to address this issue. The split design allows for crossing obstacles on one side, enabling better adaptation to the dynamic terrain of hilly and mountainous areas, ultimately maximizing the chassis' performance. Through research, it was found that the split structure effectively prevents single-sided crawler suspension, allowing for a maximum longitudinal slope angle of 42.3°, transverse slope angle of 27.38°, and a maximum ravine width of 445 mm. The prototype testing confirmed that the chassis can handle slopes of up to 41° on both sides and 30° on one side, with a maximum ravine width of 430 mm. Considering that the typical cultivated land angle in hilly and mountainous regions ranges from 2° to 15°, the designed chassis is well-suited for driving operations in underground farmland within such areas.

Keywords: hilly and mountainous machinery, split structure, crawler powered chassis, complex terrain operations, kinematic analysis

DOI: 10.25165/j.ijabe.20251803.9293

Citation: Wang W, Yuan L, Li G L, Zhang S J, Wang T J, Tang C Y. Design and experiment of split-type tracked chassis applied in hilly and mountainous regions. Int J Agric & Biol Eng, 2025; 18(3): 63–72.

1 Introduction

The hilly and mountainous regions of China cover 666 million hectares, representing 69.4% of the total land area[1]. The challenging agricultural landscape in these areas is characterized by small land parcels, diverse crop varieties, high operational risks, and a lack of mechanized farming infrastructure, which has hindered the adoption of large and medium-sized agricultural machinery. Consequently, the level of agricultural mechanization in these regions has historically been lower compared to that in flat areas. However, with the rapid advancements in agricultural machinery technology, there is an urgent need to improve the operational efficiency and safety of agricultural machinery[2]. In alignment with the objectives outlined in the "14th Five-Year Plan" of China, there is a strong momentum toward increasing the level of agricultural mechanization in hilly and mountainous regions. To achieve this, it is essential to conduct research on the walking mechanisms of crawler chassis in these terrains and investigate the effects of key structural parameters on performance.

Research on chassis designed for hilly and mountainous machinery has its origins in military applications, particularly, when Germany pioneered the development of tank chassis tailored for such terrains[3]. In the agricultural sector, advanced nations have taken the lead in investigating specialized conditions prevalent in hilly and mountainous regions. This inquiry has gradually facilitated the evolution of terrain tractors into specialized chassis designs[4,5]. Notably, the American John Deere Company is at the forefront of agricultural machinery research and design, having developed a wheat combine harvester equipped with automatic leveling capabilities on its crawler chassis[6]. This innovation features a rotary universal leveling device that allows for adaptation to the complex terrains found in hilly areas. Additionally, the research laboratory of the Georgian Academy of Agricultural Sciences contributed by designing a small, flexible tractor that is well-suited for multi-slope road operations, capable of handling a maximum operating slope of 40°[7]. However, the manual operation of this tractor is labor-intensive, potentially leading to driver fatigue and safety risks. In contrast, Japan's small crawler transport vehicles are designed for short-distance transportation across fields, slopes, and forests. These vehicles can carry loads ranging from 400 to 700 kg, with power outputs between 3.1 and 5.7 kW. They feature three forward gears, two reverse gears, and the ability to tilt the carriage for unloading, and are available in both manual and hydraulic variants, capable of navigating a 15° slope.

Compared with other countries, China's research on agricultural machinery chassis for hilly and mountainous areas started late. However, recent years have witnessed significant investments in manpower, materials, and finances dedicated to the development of agricultural machinery. Numerous enterprises and universities have engaged in extensive research on mechanical

Received date: 2024-08-19 **Accepted date:** 2025-04-20

Biographies: Wei Wang, Professor, research interest: intelligent agricultural equipment for forest fruit production, Email: syww@syau.edu.cn; **Lin Yuan**, MS, research interest: intelligent agricultural equipment for forest fruit production, Email: 15004673130@163.com; **Guolong Li**, MS, research interest: intelligent agricultural equipment for forest fruit production, Email: 2023240018@edu.syau.edu.cn; **Shiji Zhang**, MS, research interest: intelligent agricultural equipment for forest fruit production, Email: 2022240046@edu.syau.edu.cn.

†These authors contributed equally to this work.

***Corresponding author: Tiejun Wang**, PhD, Associate Professor, research interest: agricultural biosystems engineering, College of Engineering, Shenyang Agricultural University, Shenyang 110866, China. Tel: +86-18640030216, Email: tiejunwang@syau.edu.cn; **Chuanyin Tang**, PhD, Associate Professor, research interest: vehicle dynamics and control, College of Mechanical Engineering and Automation, Northeastern University, Shenyang 110819, China.Tel: +86-15040067546, Email: monsigor@aliyun.com.

chassis tailored for hilly and mountainous regions[8-12]. He et al.[13] introduced a fully hydraulic crawler chassis designed to address the limitations of traditional agricultural machinery, which often struggles to navigate complex terrains such as mountains. Wang et al.[14] developed a powered chassis equipped with triangular crawler tracks specifically for orchard operations in hilly areas, which offers low production costs but encounters challenges related to uneven mass distribution and vibrations. Han et al.[15,16] designed an orchard transportation machinery chassis capable of adjusting the transport box according to the terrain, facilitating movement on slopes of up to 10°. However, this design faces challenges due to a high mechanical load and relatively slow driving speed.

Currently, research in China regarding crawler chassis for hilly and mountainous machinery primarily focuses on theoretical analysis and prototype development. As illustrated in Figure 1, when a traditional crawler chassis encounters a single-sided wheel train on a slope, one side of the chassis becomes suspended due to its rigid structure. This phenomenon is unsuitable for hilly and mountainous terrains, as the resulting suspended movement leads to significant amplitude, which hinders transportation and operation. Furthermore, the continuous fluctuation of terrain in these areas exacerbates the suspension amplitude over time, resulting in accelerated wear and tear of the chassis and a reduced service life.

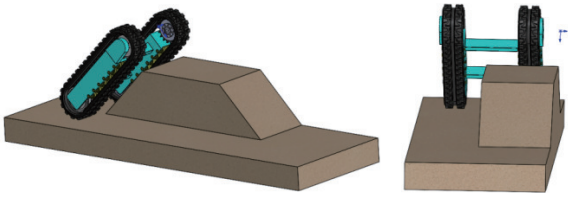

Figure 1 Traditional crawler track with one suspended in the air

This article presents the design of a crawler-type power chassis specifically tailored for agricultural machinery operating in hilly and mountainous regions, featuring a split structure. By effectively addressing the challenges posed by uneven terrain, this design prevents one side of the crawler from becoming suspended in the air, thereby facilitating smooth operation in complex environments. The research offers valuable insights that contribute to the advancement of agricultural machinery suited for hilly and mountainous areas.

2 Design of split type chassis

2.1 Split movement ideas

The traditional chassis, referred to as the integral type, maintains structural integrity during movement, whereas the split type is capable of unilateral decomposition and autonomous navigation across challenging terrains. The primary differences between integral and split types are illustrated in Figure 2. An integrated vehicle can be conceptualized as a square block, with its structural configuration remaining unchanged as it moves from point A to point B. In contrast, a split vehicle consists of the main chassis body as one component (Part 2) and the wheel assemblies on either side as separate components (Parts 1 and 3). As the split vehicle transitions from point A to point B, its structural configuration can be categorized into various combinations, such as 12 and 3, 1 and 23, or 123. Unlike the integral type, the split type incorporates distinct moving parts that collaborate during movement, thereby emphasizing the fundamental differences between the two chassis types.

The split design effectively addresses the challenge of a one-sided wheel train being suspended in mid-air while a vehicle's chassis traverses hilly and mountainous terrain, characterized by a slope on one side and flat ground on the other. In this scenario, the chassis structure is divided into two components: one component, the wheel train, ascends alongside the car body, while the other component advances on the flat surface. The control system regulates the speed to prevent any deviation and ensure a smooth passage through the varying terrain.

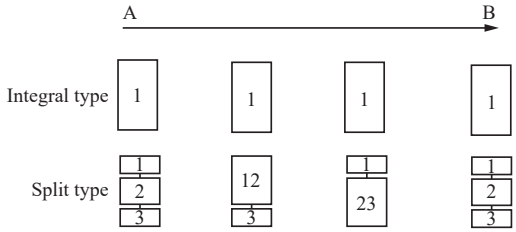

Figure 2 Schematic diagram of the difference between integrated chassis and split chassis

2.2 Design specifications

Due to the complex and variable terrain found in hilly and mountainous areas, combined with the prevailing agricultural operational methods, the use of large-scale machinery in such environments is often inefficient or occasionally unfeasible. The small agricultural machinery currently available on the market predominantly relies on fuel-powered engines, necessitating manual operation, which is labor-intensive and poses significant risks. To address these challenges, this article proposes the design of a small crawler chassis with split tracks specifically tailored for hilly and mountainous regions. The crawler chassis platform is engineered to support specific loads, typically including portable operating equipment such as manipulators, pan-tilt units, sensor module groups, and similar devices. The detailed design specifications can be found in Figure 3.

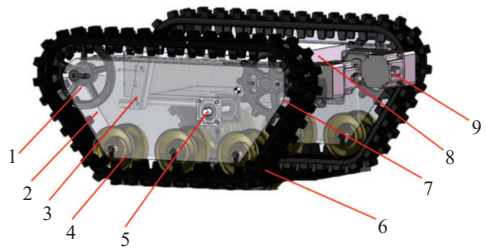

1. Tensioner wheel 2. Track wheel frame 3. Slide 4. Load-bearing wheel 5. Rotating rod 6. Track 7. Driving wheel 8. Car body 9. Motor

Figure 3 Whole machine design drawing

The entire vehicle features a symmetrical structure. Following a fundamental terrain survey and data collection, the design parameters for the chassis must comply with the requirements specified in Table 1.

Table 1 Main design indicators of chassis

Parameter	Value
Chassis quality/kg	≤ 200
Overall dimensions/mm	≤1000×1000×1000
Load weight/kg	≤50
Flat road driving speed/(km·h^{-1})	≥1
Working environment	Cement and dirt roads
Endurance/h	≥2
Climbing angle/(°)	≥15

2.3 Main structural design and selection

2.3.1 Track wheel train design and component selection

The chassis motor model[17] selected for the design index requirements is the 110BM0630-48-Z DC brush-less motor, with a rated voltage of 48 V, rated current of 40 A, rated power of 1.8 kW, and rated speed of 3000 r/min. The motor has a rated torque of 6 N·m, and is paired with an NV50 worm gear reducer with a reduction ratio of 1:50. The walking system utilizes gear-type rubber tracks, with relevant parameters calculated using a classic equation. These parameters are listed in Table 2.

Table 2 Main parameters of rubber tracks

Parameter	Value
Claw height/mm	15
Thickness/mm	20
Width/mm	150
Pitch/mm	55
Ground length/mm	750

The number of teeth on the drive wheel is a crucial parameter, with it being important for the number to be an odd and prime number in relation to the number of tracks. This ensures that each tooth on the drive wheel can properly mesh with the track spikes[18]. Following these guidelines, the number of teeth on the drive wheel was chosen to be 13. The calculation for the diameter of the drive wheel is:

$$D = \frac{t_0}{\sin(180^\circ/n)} \tag{1}$$

where, D is drive wheel diameter, mm; t_0 is track pitch, mm; n is the number of drive wheel teeth.

After calculation, a diameter of approximately 160 mm (D≈ 160 mm) was determined. The design of other crawler wheel trains follows basic design principles, with the data results presented in Table 3.

Table 3 Main parameters of the gear train

Parameter	Value
Bearing wheel radius/mm	50
Bearing wheel width/mm	25
Tensioner radius/mm	160
Tension pulley width/mm	30

The selection of a power source is critical, particularly in light of the "dual carbon plan". Traditional diesel and gasoline chassis were deemed unsuitable, prompting the adoption of an electric drive for this design. Batteries are available in various types, generally classified as alkaline or acid based on the electrolyte used. Alkaline batteries typically utilize a potassium hydroxide aqueous solution as the electrolyte. Notable examples of alkaline batteries include zinc-manganese, cadmium-nickel, and nickel-hydrogen batteries. Ultimately, the design emphasizes adherence to the required specifications, resulting in the choice of a high-strength, specialized lithium battery with a capacity of 60 V and 100 A·h.

2.3.2 Split design

The split design involves placing the end of the rotating rod in the slideway and allowing the bearing to slide along it. The initial position ensures the vehicle is level, with a horizontal line connecting the center points of the seat bearing and the bearing in the slideway. When the single-sided crawler wheel train climbs uphill, the bearing on the stressed side slides along the slide track in an arc path from A to B, causing the seat bearing on that side to rotate. The seat bearing on the other side and the bearing in the slideway remain unchanged.

Based on the principles of structural design and mounting stability, the optimal installation position for point O of the seat bearing, which facilitates rotation between the vehicle body frame and the rotating rod, is determined to be at half the height of the vehicle. Points O and A should be positioned at the maximum width of the vehicle body. At the trisection point, the length of OA measures 300 mm. Research conducted on the predominant land angles in hilly and mountainous regions of the country suggests that selecting a limit value of 45° for α can effectively address all angle-related issues in current agricultural production. Under this scenario, the chassis structure can achieve a maximum split angle of 45°, irrespective of environmental conditions. Furthermore, OB, which represents the length of OA following a positional change, also measures 300 mm. Utilizing the principles of isosceles triangle calculation, the length of AB is determined to be 229.61 mm.

In the split state, the rotating shaft is subjected to torque T, and the calculation Equation is:

$$T = G \cdot \cos\alpha \tag{2}$$

where, T is torque, N·m; G is the gravity when the chassis is separated, N; α is the movement angle, (°).

Calculated according to Equation (2), the weight at this state is the sum of the single side track and the vehicle body, the torque in the 45° limit state is 748.4 N·m.

As shown in Figure 4, according to the design content of the whole machine, the l_4 is 560 mm and the l_5 is 300 mm. The value of l_2 is related to the torque and material stress.

$$T = \tau \times \left(\frac{l_2}{17.2}\right)^3 \tag{3}$$

The material chosen for the shaft is 40Cr, with τ of 55 MPa. Substituting this value into Equation (3) yields l_2=19.25 mm, which is then rounded for optimization. The shaft diameter is set at 20 mm. Based on this diameter and other relevant data, the seat bearing model UCFU204 is selected, with inner dimensions of 20 mm, outer dimensions of 47 mm, and a width of 31 mm. Additionally, the lengths of l_1 or l_3 are determined to be 30 mm. The rolling bearing model chosen for the slideway is the 6200 deep groove ball bearing, with inner dimensions of 10 mm, outer dimensions of 30 mm, and a width of 9 mm.

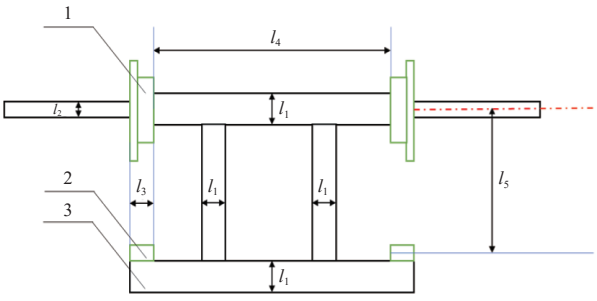

1. Seat bearing 2. Rotating rod end bearing 3. Rotating rod

Figure 4 Shaft structure diagram

The installation position of the slideway can be determined by referencing Figure 5. The design of the slideway consists of a limit track that aligns with the movement of the split structure. Specific parameters are calculated based on the guidelines provided in Figure 6.

The inclination angle of the slide is the tangent line of the arc drawn by the split structure.

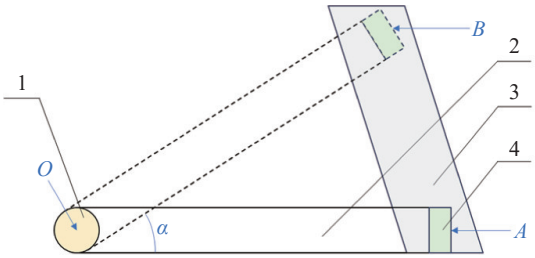

1. Seat bearing 2. Rotating rod 3. Slideway 4. Rotating rod end bearing

Figure 5 Simple diagram of unilateral process movement

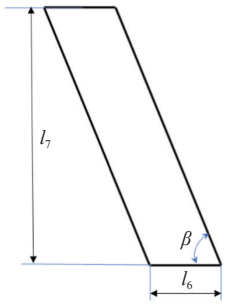

Figure 6 Slide structure diagram

$$\beta = \frac{180 - \alpha}{2} \tag{4}$$

Bringing in relevant data, the β is 67.5°. According to the angle, the length of l_6 is 30 mm and the length of l_7 is 260 mm after relevant calculations.

When encountering a single-side slope or a single-side ravine, this design implements a split movement mode, as depicted in Figure 7. Initially, the crawler train is considered as a whole entity. As it comes into contact with changes in terrain on one side, the chassis undergoes split movement due to passive terrain reaction forces. This movement involves one side of the track wheel train operating independently while the other two parts remain integrated.

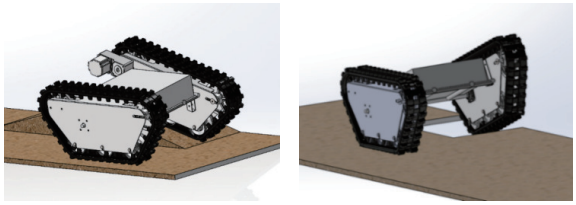

a. Instantaneous state of splitting when just entering the slope

b. Instantaneous state of separation when entering the ravine

Figure 7 Instantaneous diagram of split movement of one-sided crossing of slope and one-sided crossing of ravine

The movement mode of the chassis varies under different terrains. When a single-sided crawler train passes through a slope, it goes through three stages of change: (a) Upon entering the slope, the bearing on the slope side follows an arc trajectory from point *A* to point *B* along the slide, rotating in the process. The other side seat bearing and the bearing in the slideway remain unchanged. (b) When moving gently on a slope, both tracks are kept level with the ground. (c) Transitioning from a slope to flat ground, the bearing on the non-slope side slides along an arc trajectory from A to B, rotating in the process.

The other side seat bearing and the bearing in the slideway remain unchanged. The discussion above focuses on the movement changes of a crawler chassis passing through a single-sided slope with a split design. Contrary to the slope scenario, when the single-sided crawler train passes through a ravine, it also undergoes three stages of change: (a) Upon entering the ravine, the bearing on the opposite side of the ravine follows an arc trajectory from A to B along the slideway, with the seat bearing on the non-ravine side rotating. The other side seat bearing and the bearing in the slideway remain unchanged. (b) When smoothly passing through ravines, both crawler tracks should remain level with the ground. (c) Transitioning from the ravine to flat ground, the bearing on the ravine side slides along the arc track from *A* to *B*, rotating in the process. The other side seat bearing and the bearing in the slideway remain unchanged.

2.3.3 Machine parameters

Based on the above content, the parameter design of the whole machine is completed, and the final structural parameters of the prototype are determined (Table 4).

Table 4 Structural parameters of chassis design

Parameter	Value
Machine size (length×width×height)/mm	900×800×450
Machine quality/kg	180
Design maximum split angle/(°)	45
Drive mode	Electric

3 Theoretical analysis of chassis in different states

3.1 Flat earth kinematics and turning radius analysis

In hilly and mountainous regions, the adhesion of crawler chassis enhances the ability of mechanical equipment to navigate uneven terrains, ensuring stable traction and preventing slipping and skidding. This ultimately improves work efficiency and outcomes. Moreover, on slopes, traction adhesion disperses weight and increases friction, resulting in more dependable traction. This allows agricultural machinery to operate safely on slopes, reducing risks such as landslides and overturns.

The traction force F of the chassis is usually provided by two parts, and the calculation equation is:

$$F = F_1 + F_2 \tag{5}$$

where, F_1 is the friction force between the track support surface and the soil surface, N; F_2 is the reaction force generated by the squeezing of the track surface during the movement of the chassis, N.

An important parameter standard for the passing ability of the chassis on flat ground is the ground contact pressure P of the track. The calculation equation is as follows:

$$P = \frac{G}{2bL} \tag{6}$$

where, P is the track ground pressure, kPa; b is the track width, m; L is the track ground length, m.

The specific pressure P of the track's grounding is calculated to be 5.896 kPa, with the corresponding reaction force denoted as F_2. In addition to linear motion, the crawler chassis also incorporates steering motion. When a crawler vehicle turns and moves, the contact between the tracks and the ground generates significant frictional resistance, impacting the selection of the drive motor and obstacle-crossing stability analysis. Therefore, analyzing the steering of the crawler chassis is crucial[19,20]. The steering of the crawler chassis involves rotational movement around a specific point. It utilizes the difference in rotational speed of the drive motors to steer, determining the turning radius. Since the crawler chassis operates at low speeds, the impact of centrifugal force is not

taken into account in the steering analysis. Figure 8 illustrates a schematic diagram of the crawler vehicle's steering mechanism.

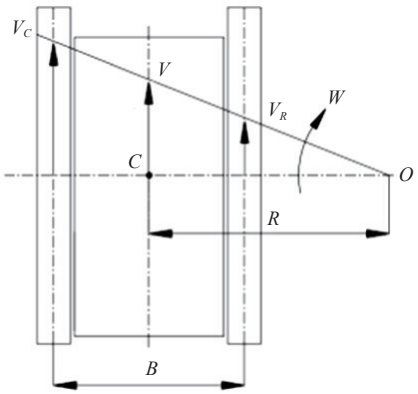

Figure 8 Track chassis steering diagram

In the plane, the center of rotation for the crawler vehicle's running mechanism is denoted as O, with the centerfold position of the crawler vehicle marked as point C. The uniform rotation radius of the crawler vehicle's running mechanism around point O is represented as R, which is the length between points O and C. The center distance of the crawler track of the chassis is noted as B. When the crawler vehicle's crawler undergoes steering movement at an angular speed, the linear speed of the steering mechanism on the left side of the crawler vehicle is v_L, while the linear speed of the steering mechanism on the right side is v_R. The expressions for linear velocity v_L and v_R are as follows:

$$\begin{cases} v_L = (R - 0.5B)\omega \\ v_R = (R + 0.5B)\omega \end{cases} \tag{7}$$

The assumption is that the driving wheel of the traveling mechanism is fully engaged with the crawler, ensuring that the linear speed of the crawler running mechanism remains consistent and equal in magnitude to the direction of the crawler driving wheel. Representing the angular velocity of the driving wheels on the left and right sides as ω_L and ω_R respectively, the equation for the radius of rotation R can be expressed as:

$$R = \frac{0.5B(\omega_L + \omega_R)}{\omega_L - \omega_R} = 0.5B\left(1 + \frac{2}{\frac{\omega_L}{\omega_R} - 1}\right) \tag{8}$$

The relationship between the rotation radius and the changes in left and right crawler speed was analyzed using MATLAB software to draw an equation, as shown in Figure 9.

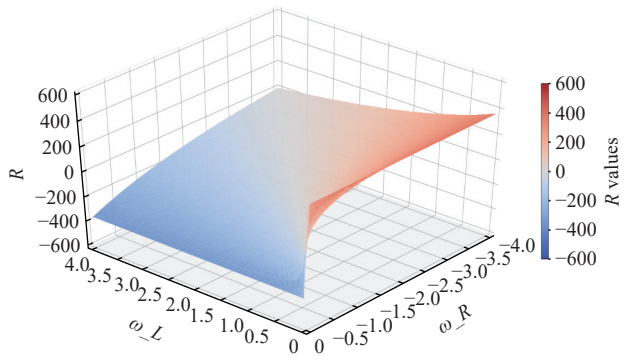

Figure 9 Change diagram of the relationship between rotation radius and left and right crawler speeds

The relative rotation radius ρ can be obtained according to Equation (9):

$$\rho = \frac{R}{B} \tag{9}$$

Figure 10 illustrates how the steering characteristics of a tracked vehicle are determined by the value of ρ. When $\rho > 1/2$, the angular speed ratio of the two driving wheels in the crawler vehicle's mechanism is $\omega_L/\omega_R > 1$, causing the vehicle to always rotate to the right whether moving forward or backward. As ω_L/ω_R approaches 1, ρ approaches infinity, resulting in an infinite rotation radius R where the vehicle moves in a straight line. When $\rho = 1/2$, ω_L/ω_R tends towards infinity, indicating a rotational motion around the center of the right running mechanism with a rotation radius of $0.5B$. For $0 \leq \rho < 1/2$, the tracked vehicle rotates in place around the chassis centroid when ω_L and ω_R have the same magnitude but opposite directions.

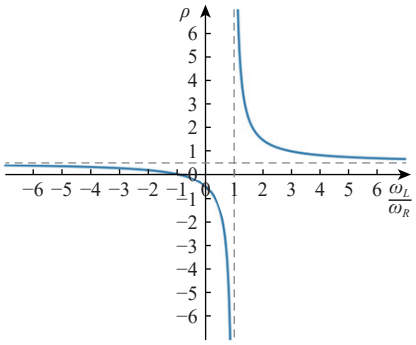

Figure 10 Relationship between the relative rotation radius ρ and the left and right crawler speed ratio

3.2 Slope kinematics analysis

3.2.1 Analysis of slope stability and maximum slope angle

(1) Longitudinal slope

When stationary on a longitudinal slope, the force diagram of a mountain crawler chassis in the longitudinal plane is depicted in Figure 11. Here, O_1 represents the trailing edge of the track support surface, α denotes the slope angle, L signifies the chassis track grounding length, a indicates the horizontal distance from the chassis center of gravity to O_1, h_g represents the height of the chassis center of gravity, and X represents the horizontal distance from N to O_1. Since the chassis is not in motion, there is no rolling resistance or rolling resistance moment. The forces acting on the mountain crawler chassis include the chassis gravity G, the total vertical reaction force N on the ground facing the crawler support section, and H and V as the components of the chassis gravity G parallel and perpendicular to the slope plane.

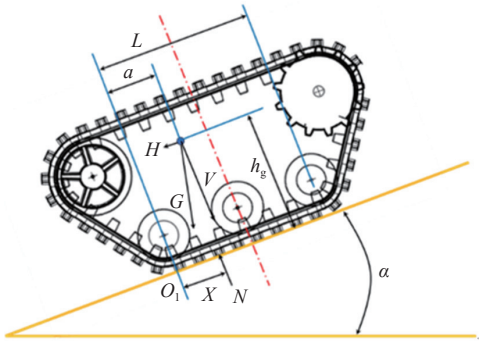

Figure 11 Force diagram of mountain crawler chassis in the longitudinal plane

Upon analyzing the stress exerted on the crawler chassis while navigating the longitudinal slope, the moment of O_1 can be calculated using the moment balance equation.

$$\sum M_{0_1} = 0 \tag{10}$$

$$N \cdot x + H \cdot h_g - V \cdot a = 0 \tag{11}$$

The vehicle's gravity is divided into components based on the system, and the equation for the converted components is derived.

$$\begin{cases} H = G\sin\alpha \\ V = G\cos\alpha \end{cases} \tag{12}$$

The equilibrium equations are obtained after banding:

$$G\cos\alpha \cdot x + G\sin\alpha \cdot h_g - G\cos\alpha \cdot a = 0 \tag{13}$$

To prevent tipping when stationary on an uphill slope, the condition is that the vertical reaction forces from the ground facing the crawler support section must not fall behind the trailing edge of the crawler support surface.

$$\alpha \le \arctan\left(\frac{a}{h_g}\right) \tag{14}$$

When the crawler chassis is stationary uphill, a smaller center of gravity height h_g results in a greater distance a from the center of gravity to the trailing edge of the crawler support section. Additionally, a larger α angle reduces the likelihood of tipping over.

Figure 12 illustrates the center of mass of the chassis and the center of the load-bearing wheel. Based on the relevant data, when the angle is 15°, the chassis will not tip over as the inequality condition is met. The maximum passing angle without tipping over is calculated to be 42.37°.

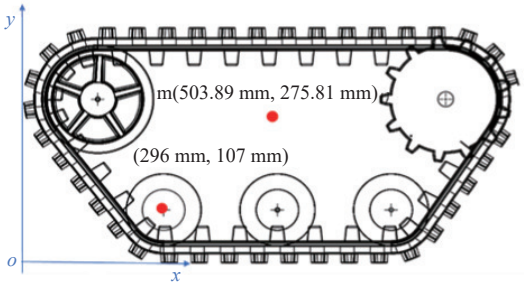

Figure 12 Schematic diagram of center of mass position

(2) Transverse slope

When the chassis is completely on a transverse slope, the stress throughout the structure differs from that on a longitudinal slope. A stress analysis is conducted considering the relevant forces and the position of the center of mass, as depicted in Figure 13.

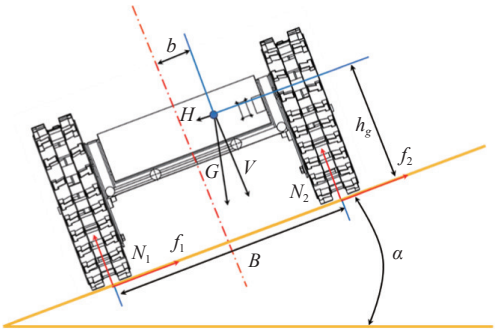

Figure 13 Force analysis on transverse slopes

In Figure 13, O represents the center of mass, α denotes the angle value of the transverse slope, b indicates the offset between the center of mass and the longitudinal center section of the chassis, and N_1 and N_2 are the support forces exerted by the ground. Additionally, f_1 and f_2 represent the friction forces between the ground and the track.

$$\alpha = \arctan\frac{0.5B + b}{h_g} = \arctan\frac{B}{2h_g} \tag{15}$$

When the chassis is driving on roads with challenging conditions, if the slope angle surpasses a certain limit, the vehicle may slide towards the side with lower traction, leading to either overall slippage or tipping. In order to determine this critical angle, specific equations must be developed and analyzed.

$$N_2 B - G\cos\alpha(0.5B + b) + Gh_g\sin\alpha = 0 \tag{16}$$

$$N_2 = \frac{\left[G\cos\alpha(0.5B + b) - Gh_g\sin\alpha\right]}{B} \tag{17}$$

When N_2=0, rollover will occur, and α is the maximum critical value at this time. Since the load status is not considered in the analysis at this time, the center of mass position is the standard position. Therefore, b=0. Putting the designed chassis-related design data into Equation (18), the maximum lateral slope is 27.38°.

$$\alpha_{\max} = \arctan\frac{0.5B + b}{h_g} = \arctan\frac{B}{2h_g} \tag{18}$$

3.2.2 Analysis of torque, stress, and shaft deformation under unilateral slope movement

The analysis given above applies to the stability and maximum angle analysis of both single-sided slope crossing and double-sided slope crossing. In the case of single-sided slope crossing, there will be a relative twisting effect when the rotating shaft rotates. The specific movement pattern of single-sided slope crossing is illustrated in Figure 14.

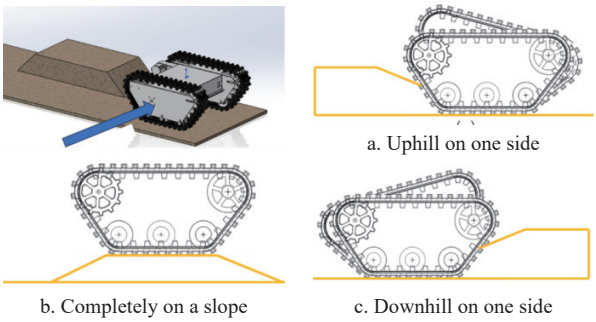

Figure 14 Schematic diagram of one-sided slope crossing

In the above process, the shaft twists in both state (a) and state (c) and is affected by torsion (Figure 15).

$$\sum M_e = 0 \tag{19}$$

$$T - M_e = 0 \tag{20}$$

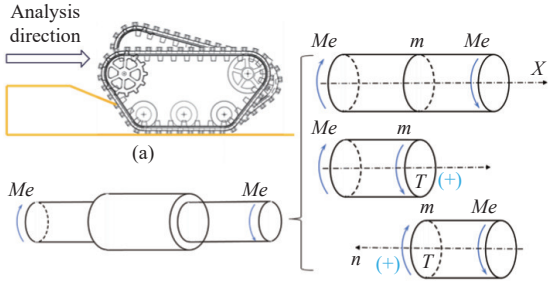

Figure 15 Torque analysis diagram

$$T = M_e \tag{21}$$

According to Equation (21),

$$M_e = G \cdot \cos\alpha = T \tag{22}$$

where, α represents the angle of the slope on one side, and g is 9.8 N/kg. According to the calculation, T=781.94 N·m in this state can be obtained. The maximum stress on this axis is calculated using the cross-section method, and the physical quantity analysis is as shown in Figure 16.

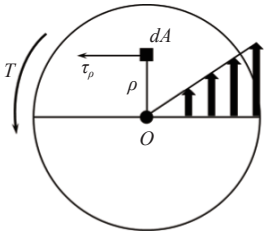

Figure 16 Cross-sectional analysis

According to the definition, the moment of the internal force system about the center of the circle is the torque on the cross section.

$$\begin{cases} T = \int_A \rho\tau_\rho \mathrm{d}A \\ I_\rho = \int_A \rho^2 \mathrm{d}A \end{cases} \tag{23}$$

According to Hooke's law of shear, the equation of shear stress τ_ρ at a distance ρ from the center of the circle is as follows:

$$\tau_\rho = \rho G' \frac{\mathrm{d}\varphi}{\mathrm{d}x} \tag{24}$$

When ρ is equal to the section radius, the shear stress is maximum.

$$\tau_{\max} = \frac{T}{W_\rho} \tag{25}$$

$$W_\rho = \frac{\pi D^3}{16} \tag{26}$$

where, W_ρ is the torsional section coefficient, m^3; D is the cylinder diameter of solid shaft, m.

When the cross-section radius r_A=r_C=0.02 m and r_B=0.03 m, the segmental shear stress is 49.8MPa in sections A and C and 13.07 MPa in section B. The design material is 40Cr alloy steel, which [τ]=55 MPa, $\tau_{\max}$≤[τ].

According to the basic equation of torsional deformation,

$$\varphi = \int_0^l \frac{T}{GI_\rho}\mathrm{d}x = \frac{Tl}{GI_\rho} \tag{27}$$

As shown in Figure 17a, l_A=l_C=0.012 m and l_B=0.05 m, $I\rho$= 79 GPa. When the diameters of different sections of a circular shaft made of the same material vary, the torsion angle of each section is calculated individually, and then the algebraic values are summed.

$$\varphi = \sum \frac{T_i l_i}{GI_{\rho i}} \tag{28}$$

The final calculation shows that the deformation of the entire shaft is φ≈0.06°. The size of the shape variable in this state is sufficiently small to meet the design requirements.When in state (c), the value changes from cosα to sinα. The torsion angle of each segment is calculated according to Equation (28), and then added according to the algebraic values to get φ≈0.054°. The size of the shape variable in this state is sufficiently small to meet the design requirements.

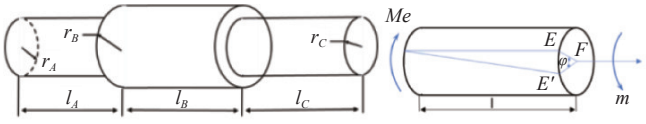

a. Parameters of each section b. Torsional deformation of each segment

Figure 17 Analysis of parameters and torsional deformation of each section of the rotating shaft

3.3 Ravine kinematics analysis

3.3.1 Maximum ravine width analysis

The stability of a tracked vehicle while crossing a ditch can be compromised by changes in posture and position. This is mainly due to the center of mass position when the vehicle first makes contact with the side of the ditch. To analyze this, a rectangular coordinate system O_1 is established with the load-bearing wheel of the crawler chassis near the driving wheel as the center of the circle, and the positive x-axis signifies the forward direction. For a tracked vehicle to safely cross a ditch, it must have its center of mass position m near the inner wall of the ditch on the left, allowing the front track of the vehicle to contact the inner wall of the right side of the ditch, as depicted in Figure 18.

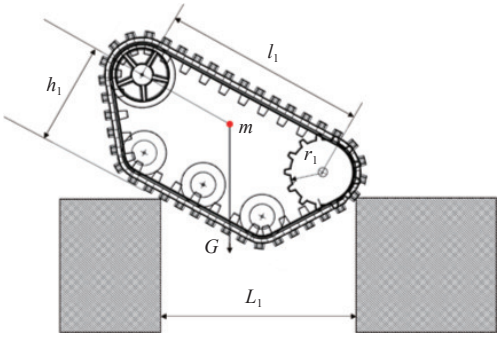

Figure 18 Simplified diagram of track chassis ravine movement

Based on the analysis based on the instantaneous method, the model can be established to obtain the calculation equation for the maximum ravine that the crawler chassis can span.

$$L_1 = \sqrt{\left(\frac{l_1}{2}\right)^2 + h_1^2} + r_1 \tag{29}$$

where, L_1 is the ravine width, mm; l_1 is the maximum wheel train width, mm; r_1 is the drive wheel radius, mm; h_1 is the load-bearing wheel center height, mm.

Relevant data is brought in according to the design content, and after calculation, the maximum width that can be spanned is 445 mm.

3.3.2 Analysis of torque, stress, and shaft deformation under unilateral slope movement

The above analysis is applicable to the maximum ravine analysis of single-sided and double-sided ravines. When the chassis passes through a single-sided ravine, the force generated by the rotation of the rotating shaft will cause relative twisting of the shaft. The specific movement pattern is shown in Figure 19.

In the above process, the axis twists in both the (a) state and the (c) state. Affected by the torsion, the analysis method is consistent with the slope.

According to the theoretical calculation, the length of the tracked vehicle across the ravine L=445 mm, and the calculated

angle between the tracked vehicle and the inside of the left side of the ravine is 54°, but the maximum angle can only be achieved at 45°.When in state (a), the magnitude of the torque at this time is calculated according to Equation (22) and angle value changes from cosα to sinα: T=748.39 N·m; the segmented shear stress τ_{max} at A, B, and C are 47.66 MPa, 14.12 MPa, and 47.66 MPa, respectively. The design material is 40Cr alloy steel, which also $\tau_{max} \leq [\tau]$. The torsion angle of each segment is calculated according to Equation (28), and then added according to the algebraic values to get $\varphi \approx 0.0586°$. In summary, the shape variable of this axis in this state is very small and can meet the design requirements.

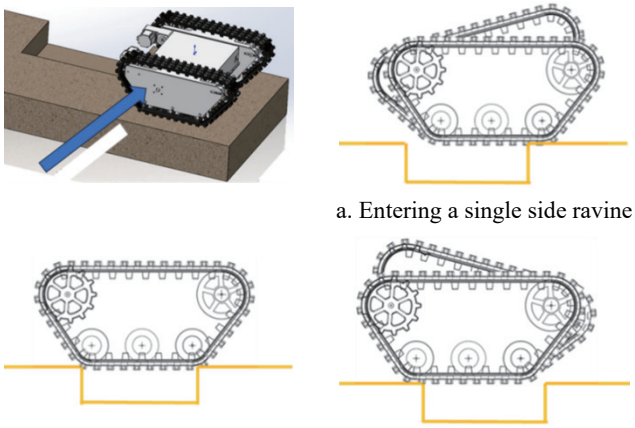

a. Entering a single side ravine

b. Passage a single side ravine c. Leaving a single side ravine

Figure 19 Unilateral groove movement process diagram

When in state (c), the magnitude of the torque at this time is calculated according to Equation (22): T=748.39 N·m; the segmented shear stress τ_{max} at A, B, and C are 47.66 MPa, 14.12 MPa, and 47.66 MPa, respectively. The torsion angle of each segment is calculated according to Equation (28), and then added according to the algebraic values to get $\varphi \approx 0.0586°$. In summary, the shape variable of this axis in this state is very small and can meet the design requirements.

4 Test of split crawler power chassis

4.1 Prototype production

The parts of the crawler chassis are processed and assembled based on the three-dimensional structural design. The prototype of the crawler chassis is depicted in Figure 20. Following the layout of component locations, the design of software, hardware, and control system for the crawler chassis is finalized. Subsequently, a stability test is carried out to validate the theoretical derivation.

Figure 20 Split crawler chassis prototype

Currently, control platforms for tracked vehicles are typically categorized into three types: autonomous, semi-autonomous, and remote control[21-23]. The future trajectory for control methods leans towards autonomy, although current autonomous control methods are not yet fully developed. The hardware required for autonomous control is costly, with most systems still in the testing phase. As a result, remote control remains the most prevalent and dependable method of control. The proposed crawler chassis will be operated via remote control, with the machine's operation depicted in the accompanying Figure 21.

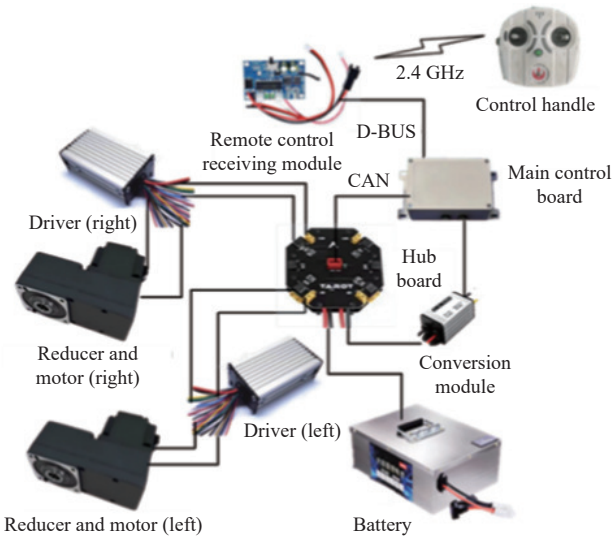

Figure 21 Control wiring diagram

4.2 Chassis passes slope test

To simulate the real environment, an artificially constructed test site is used. For the measurement of the slope angle, a special slope measuring ruler for civil engineering is used for measurement. The test environment of the chassis for field prototype testing is as shown in Figure 22.

a. Measurement of slope angle b. Slope test environment

Figure 22 One-sided and two-sided passage through the slope test site

When passing through slopes on both sides, the screenshots of each status are as in Figure 23.

The three stages (a)-(c) respectively correspond to the three stages of theoretical analysis. The final test of passing through the terrain at a constant speed shows that the maximum angle that can be passed on both sides in a stable state is 41°. Different from the two sides, when passing through the slope on one side, the various shapes are as shown in Figure 24.

The three stages (a)-(c) correspond to the three stages of theoretical analysis, respectively. Maintaining a constant speed through the terrain, the final test shows that the maximum angle that can be passed on one side in a stable state is 30°.

4.3 Chassis passes ravine test

To simulate the real environment, an artificially constructed test site is used. For the measurement of the slope angle, a special slope measuring ruler for civil engineering is used for measurement. The chassis is subjected to field prototype testing. The testing environment is as shown in Figure 25.

a. Bilateral uphill slopes b. Completely on a slope c. Bilateral downhill slopes

Figure 23 Bilateral slope test

a. Uphill on one side b. Completely on a slope c. Downhill on one side

Figure 24 Unilateral slope test

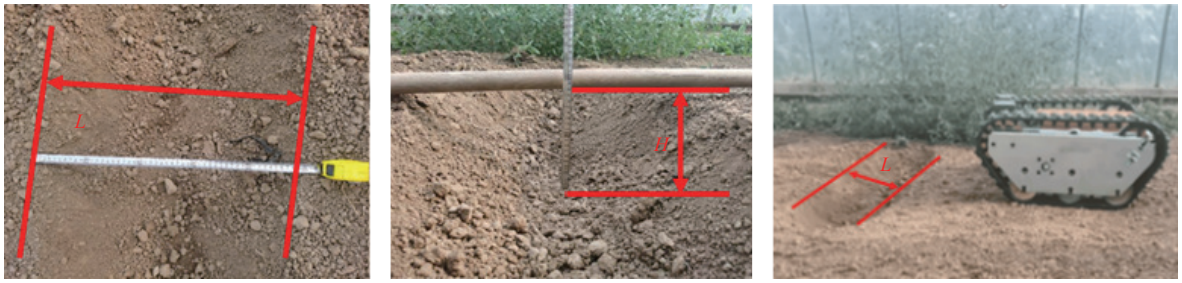

a. Measuring ravine width b. Measuring ravine depth c. Ravine test environment

Figure 25 Unilateral and bilateral passage through ravine test site

When passing through a ravine on both sides, the various states are as shown in Figure 26.

The three stages (a), (b), and (c) respectively correspond to the three stages of theoretical analysis. Maintaining a constant speed through the terrain, the final test showed that the maximum ravine width that can be passed on both sides in a stable state is 430 mm. When passing through a ravine on one side, the various states are as shown in Figure 27.

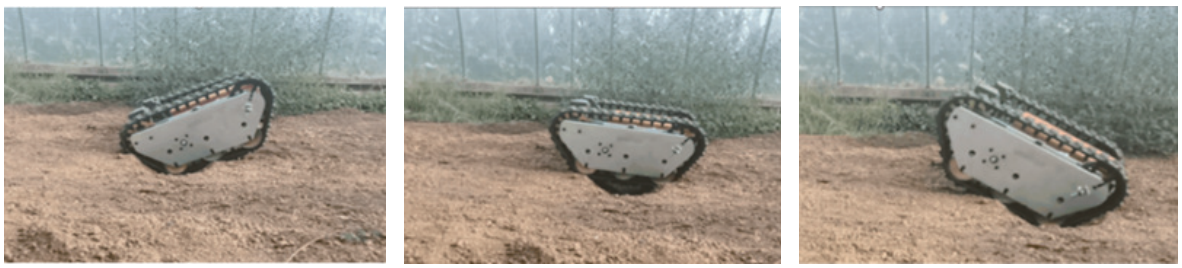

a. Entering bilateral ravine b. Passage bilateral ravine c. Leaving bilateral ravine

Figure 26 Bilateral ravine crossing test

a. Entering a single side ravine b. Passagea single side ravine c. Leaving a single side ravine

Figure 27 Unilateral ravine crossing test

The three stages (a), (b), and (c) respectively correspond to the three stages of theoretical analysis. Maintaining a constant speed through the terrain, the final test showed that the maximum ravine width that can be passed on both sides in a stable state is 430 mm. After multiple repeated experiments, the tracked vehicles were able to pass through the aforementioned road conditions without any issues. In addition to testing the traditional road conditions mentioned earlier, tests were also conducted on grass and cement roads. The crawler chassis was able to pass through these conditions smoothly, demonstrating excellent performance.

5 Conclusions

To address the issue of the chassis remaining elevated on one side after traversing an obstacle in the complex terrain of hilly areas, this article proposes a split-type design and develops a crawler chassis specifically suited for mountainous environments. It establishes standards for the overall structure and design while selecting appropriate components for the crawler vehicle. Theoretical analyses and calculations were conducted to evaluate the stability of the designed tracked vehicle under various road conditions, utilizing classic road scenarios for this purpose. Subsequently, a prototype was fabricated for experimental validation. The final conclusions are as follows:

1) A crawler chassis based on a split structure has been designed. This design effectively addresses the one-sided suspension issue that arises when the chassis traverses mountainous terrain.

2) The stability and deformation of the rotating shaft of the tracked vehicle are analyzed under slope and ravine road conditions. Three classic road conditions are selected for this analysis: flat, sloped, and ravine. The attitude changes of the tracked vehicle are planned for each condition, and the theoretical maximum capabilities of the chassis are determined through an obstacle-crossing mechanism analysis. The findings indicate a maximum slope of 42.3° and a maximum passable ravine width of 445 mm. Following an assessment of the stress and deformation of the rotating shaft under various conditions, it is concluded that the selected material meets the design requirements.

3) The crawler vehicle prototype is then assembled, and a control system is established. Actual measurements are conducted on the prototype, which includes tests for crossing ravines and climbing slopes. The test results demonstrate that the prototype can navigate a maximum slope of 41° and a maximum ravine width of 430 mm. Overall, the designed inverted trapezoidal crawler chassis largely fulfills the previously established technical specifications and meets practical application needs.

Developing a crawler chassis for mountain operations is a complex systems engineering endeavor. While the current research has made notable progress, further resources and manpower are necessary for more comprehensive exploration. It is important to note that this article focuses solely on the strength of the shaft without conducting a fatigue analysis. By developing a high-performance crawler track to replace manual labor, this research aims to contribute to societal advancement.

Acknowledgements

The authors acknowledge that this work was financially supported by the Basic Scientific Research Project of the Education Department of Liaoning Province (Grant No. LJ212410157007).

[References]

[1] Gao Q M, Pan D, Zhang X. Design and simulation of full-track modular unmanned agricultural power chassis. Transactions of the CSAM, 2020; 51(S2): 561–570. (in Chinese)

[2] Zheng Y J, Jiang S S, Chen B T. Research progress on mechanization technology and equipment for orchards in hilly mountainous areas. Transactions of the CSAM, 2020; 51(11): 1–20. (in Chinese)

[3] Wang D P. Research on forecasting demand for ordnance equipment support forces in alpine mountainous areas based on queuing theory. Master dissertation. Chongqing: Chongqing University, 2012; 50p. (in Chinese)

[4] Neumann M, Predki T, Heckes. Snake-like, tracked, mobile robot with active flip pers for urban search-and-rescue tasks, Adaptive Mobile Robotics. Ind. Robot, 2013; 40(3): 246–250.

[5] Scordamaglia V, Nardi V A. A set-based trajectory planning algorithm for a network cont rolled skid-steered tracked mobile robot subject to skid and slip phenomena. Journal of Intelligent & Robotic Systems, 2021; 101(1): 1–20.

[6] Zhao E P. Kinematics and dynamics analysis of the self-adjusting mechanism of the tractor body posture in hilly and mountainous areas. Master dissertation. Jilin: Jilin University, 2018; 92p. (in Chinese)

[7] Li J J. Design and analysis of the key components of the vehicle chassis in shallow hills. Master dissertation. Yinchuan: Ningxia University, 2021; 66p. (in Chinese)

[8] Jiang Y, Sun Z Y, Wang R C. Design and performance of omnidirectional leveling system for crawler operating machines in hilly mountainous areas Experiment. Transactions of the CSAE, 2023; 39(18): 64–73. (in Chinese)

[9] Zhang W, Tuo H Z, Yi W Y, Wang P. Development status and prospects of agricultural transportation equipment in hilly and mountainous areas. Southern Agricultural Machinery, 2020; 51(11): 9–11, 17.

[10] Xing K, Zhang L, Li Z P. Design and test of twist posture adjustment device for wheeled hilly mountain tractor. Transactions of the CSAM, 2022; 53(6): 425–433. (in Chinese)

[11] Zhou B C, Chen S Y, Hu J N, You Y, Wang D C, Zhang Q. Multi-body dynamics modeling and test of an articulated steering half-track tractor. Int J Agric & Biol Eng, 2023; 16(6): 124–133.

[12] Xin Z, Jiang Q B, Zhu Z X, Shao M X. Design and optimization of a new terrain-adaptive hitch mechanism for hilly tractors. Int J Agric & Biol Eng, 2023; 16(4): 134–144.

[13] He L. Research on full hydraulic crawler chassis in hilly area. Master dissertation. Yaan: Sichuan Agricultural University, 2021; 78p. (in Chinese)

[14] Wang F, Yang L, Xie S Y, Ma Y, Zhang J, Duan T Y. A kind of triangle Design and research of crawler-type orchard power chassis. Agricultural Mechanization Research, 2019; 41(5): 91–96. (in Chinese)

[15] Han Z H, Zhu L C, Yuan Y W. Performance analysis and optimization design of crawler chassis in mountain orchards on slopes. Transactions of the CSAM, 2022; 53(5): 413–421,448.

[16] Han Z H, Zhu L C, Yuan Y W. Design and experiment of mountain orchard transport vehicle based on adaptive control of center of gravity. Transactions of the CSAM, 2022; 53(2): 430–442. (in Chinese)

[17] Zhang L. Design of twisting attitude adjustment device for wheeled hilly mountain tractors and test. Master dissertation. Taian: Shandong Agricultural University, 2022; 74p. (in Chinese)

[18] Yin C Q. Development of crawler electric chassis in hilly mountainous areas. Master dissertation. Changsha: Hunan Agricultural University, 2021; 66p. (in Chinese)

[19] Jin S. Research on dynamic characteristics of crawler transport vehicle traveling mechanism. Master dissertation. Huludao: Liaoning University of Engineering and Technology, 2021; 94p. (in Chinese)

[20] Xie X, Han X, Zhang Z. Structural design and test of arch waist dynamic chassis for hilly and mountainous areas. The International Journal of Advanced Manufacturing Technology, 2023; 127: 1921–1933.

[21] Gao Q Y, Gao M, Song L J. Research on the trajectory correction method of crawler vehicles. Chinese Journal of Engineering Machinery, 2023; 21(6): 527–531.

[22] Luka P, Ivan B. Experimental validation of a high-speed tracked vehicle powertrain simulation model. Measurement Science Review, 2023; 23(5): 192–201.

[23] Reher T, Lavaert C, Willockx B. Potential of sugar beet (*Beta vulgaris*) and wheat (*Triticum aestivum*) production in vertical bifacial, tracked, or elevated agrivoltaic systems in Belgium. Applied Energy, 2024; 359: 122679.